Current Biology 22, 1047–1056, June 19, 2012 ©2012 Elsevier Ltd All rights reserved DOI 10.1016/j.cub.2012.04.012

Article

Single-Molecule Tracking of Collagenase on Native Type I Collagen Fibrils Reveals Degradation Mechanism

Susanta K. Sarkar,[1] Barry Marmer,[2] Gregory Goldberg,[2,*] and Keir C. Neuman[1,*]
[1]Laboratory of Molecular Biophysics, National Heart, Lung and Blood Institute, National Institutes of Health, Bethesda, MD 20892, USA
[2]Department of Biochemistry and Molecular Biophysics and Division of Dermatology, Washington University School of Medicine, St. Louis, MO 63110, USA

Summary

Background: Collagen, the most abundant human protein, is the principal component of the extracellular matrix and plays important roles in maintaining tissue and organ integrity. Highly resistant to proteolysis, fibrillar collagen is degraded by specific matrix metalloproteases (MMPs). Degradation of fibrillar collagen underlies processes including tissue remodeling, wound healing, and cancer metastasis. However, the mechanism of native collagen fibril degradation remains poorly understood.
Results: Here we present the results of high-resolution tracking of individual MMPs degrading type I collagen fibrils. MMP1 exhibits cleavage-dependent biased and hindered diffusion but spends 90% ± 3% of the time in one of at least two distinct pause states. One class of exponentially distributed pauses (class I pauses) occurs randomly along the fibril, whereas a second class of pauses (class II pauses) exhibits multistep escape kinetics and occurs periodically at intervals of 1.3 ± 0.2 μm and 1.5 ± 0.2 μm along the fibril. After these class II pauses, MMP1 moved faster and farther in one direction along the fibril, indicative of biased motion associated with cleavage. Simulations indicate that 5% ± 2% of the class II pauses result in the initiation of processive collagen degradation, which continues for bursts of 15 ± 4 consecutive cleavage events.
Conclusions: These findings provide a mechanistic paradigm for type I collagen degradation by MMP1 and establish a general approach to investigate MMP-fibrillar collagen interactions. More generally, this work demonstrates the fundamental role of enzyme-substrate interactions including binding and motion in determining the activity of an enzyme on an extended substrate.

Introduction

Collagenous scaffolds, a major element of the vertebrate extracellular matrix (ECM), are deposited and remodeled by resident cells providing an organized milieu that in turn exerts multiple effects on cell activity, including differentiation and migration [1, 2]. Morphogenesis, angiogenesis, uterine involution, bone resorption, and wound healing are all characterized by intensive tissue remodeling that involves degradation of the ECM [3]. Resident cells within tissues, along with infiltrating inflammatory cells, express matrix metalloproteases (MMPs) that degrade ECM macromolecules such as collagens and proteoglycans [3–5]. The MMP enzyme family comprises secreted and membrane-associated pro-proteases that require activation [6]. The role of MMPs in both normal and pathological processes involves tissue remodeling and MMPs are implicated in pathological conditions, including atherosclerosis [7] and rheumatoid arthritis [8]. Malignant cells also exploit these enzymes to promote metastatic invasion [9, 10]. A subset of human MMPs, the collagenases (MMP1, MMP8, MMP13, and MMP14), uniquely initiate degradation of type I, II, and III fibrillar collagens, the predominant collagens in vertebrates. These enzymes cleave all three polypeptide chains of the 300 nm triple-helical collagen monomer at a specific recognition site ~225 nm from the N terminus.

Whereas the degradation of triple-helical collagen monomers has been investigated in detail by several methods [11–15], collagenolysis of native fibrils has proved difficult to study. Native collagen fibrils are insoluble, heterogeneous, and extended substrates, rendering them refractory to conventional ensemble kinetic analysis [16]. Moreover, unlike other extended substrates such as DNA and membranes, which are structurally well characterized, the organization of individual collagen monomers in a fibril is poorly understood, making the degradation mechanism more difficult to probe and degradation data more difficult to interpret. Studies on reconstituted collagen fibrils (repolymerized acid-soluble collagen) [17–20] demonstrated a dramatic ~100-fold decrease in the cleavage rate of fibrillar versus triple-helical monomeric collagen but provide few mechanistic details of fibril degradation. Interestingly, triple-helical collagen monomers have been shown to be thermally unstable at body temperature [21] and these vulnerable unfolded states of collagen monomers may play a role in collagenolysis [22]. It has been postulated that the thermal instability of collagen monomers, when assembled into a fibril, can lead to local unfolding or "breathing," making otherwise resistant fibrils vulnerable to collagenolysis [21]. Whether local unfolding or "breathing" occurs at specific locations on fibrils or at random, making fibril degradation unlike the degradation of collagen monomers, is unknown. Fluorescence correlation spectroscopy (FCS) [17, 23] approaches have been used to measure the diffusion of MMPs, including the soluble portion of the membrane-bound MMP14, on reconstituted collagen fibers and lead to a "burnt-bridge" model of collagen degradation, but lack the resolution to address the mechanistic details of the fibrillar degradation process. Single-molecule approaches have been used to address the influence of force on the rate of collagen monomer cleavage [24, 25] and to image the interactions between collagen monomers and MMPs [26, 27]. To date, however, single-molecule approaches have not been employed to measure native fibril degradation.

Here we report how MMP1 moves on and cleaves native type I collagen fibrils by tracking single molecules of fluorescently labeled MMP1 on rat tail tendon collagen fibrils by using a prism-type total internal reflection fluorescence microscope (TIRFM). Global analysis of the single-molecule tracking

*Correspondence: goldberg@dom.wustl.edu (G.G.), neumankc@mail.nih.gov (K.C.N.)

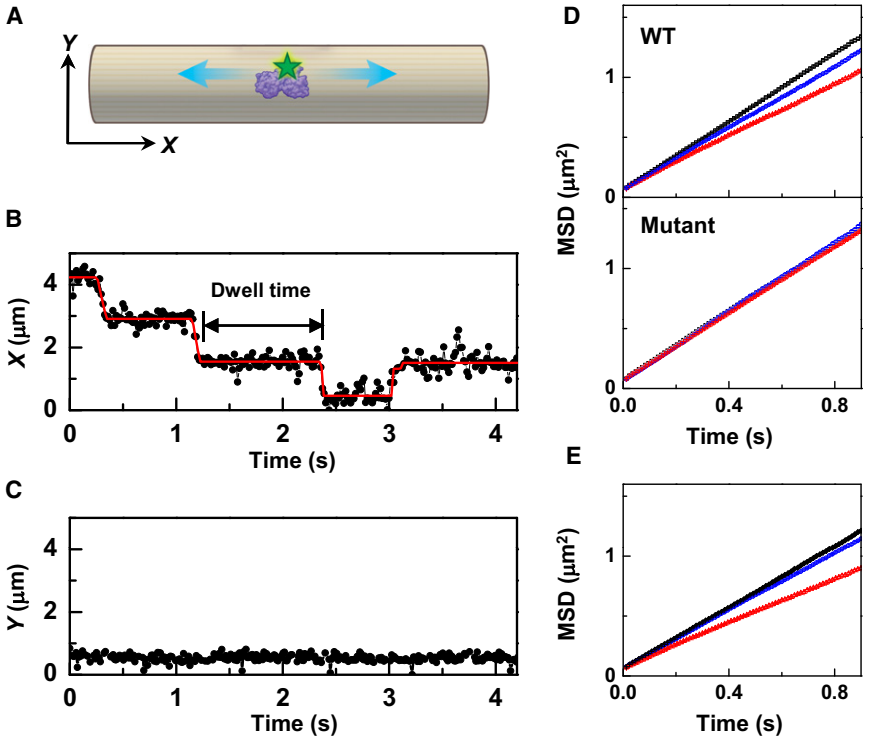

Figure 1. Tracking of Individual MMPs on a Collagen Fibril

(A) Schematic representation of the experiment (not to scale). Fluorescently labeled MMP1 (purple with green star representing fluorophore) moving on collagen fibril (beige) was tracked with a prism-type total internal reflection microscope. (B and C) MMP1 trajectories can be separated into (B) motion along the fibril (x) and (C) motion across the fibril (y). Motion along the fibril was fit to a series of runs and dwells (red line in B).

(D) Top: MSD of the motion along the fibril for WT MMP1 as a function of time at 20°C (black squares; number of trajectories, n = 1,423), 32°C (blue circles, n = 1,623), and 37°C (red triangles, n = 1,773). Bottom: The MSD for mutant MMP1 (E219Q) that binds collagen but lacks proteolytic activity. Diffusion was neither biased nor hindered at 20°C (black squares, n = 1,487), 32°C (blue circles, n = 889), or 37°C (red triangles, n = 3,663).

(E) Hindered diffusion of mutant MMP1 at 20°C after incubation with WT MMP1 at 37°C. Control reaction incubated with unlabeled mutant MMP1 at 37°C (black squares, n = 1,180), incubation with 500 pM WT MMP1 (blue circles, n = 2,087) and 1500 pM WT MMP1 (red triangles, n = 631) at 37°C for 30 min and 90 min, respectively.

Error bars in (D) and (E) represent the standard error of the mean. See also Figure S1.

records reveals that MMP1 undergoes collagenolysis-dependent biased and hindered motion on collagen fibrils. Analysis of individual trajectories shows that the motion is frequently interrupted by two classes of pauses. One class of pauses (class II) exhibit multistep escape kinetics and occur at periodic intervals along the collagen fibril at sites where MMP1 binds strongly and initiates degradation in a temperature-dependent manner. Collagen degradation was inferred from the unidirectional increase in the extent and velocity of motion immediately after the long class II pauses. To understand these data in the context of fibril architecture, we constructed a physical representation of the collagen monomer organization in a fibril. Combining the tracking data and the physical representation allowed development of a model for native collagen fibril degradation. Simulated trajectories of MMPs based on this model reproduce the salient features of the experiments and provide additional insights into MMP1 activity that could not be directly determined from the single-molecule trajectories. From these findings, we conclude that 5% ± 2% of class II pauses (long, gamma distributed, and periodically spaced) result in the initiation of collagenolysis that proceeds in a processive burst of 15 ± 4 cleavage events in rapid succession. This study provides a mechanistic paradigm of native type I collagen fibril degradation by MMP1 and establishes a general approach to study MMP-fibril interactions with other MMPs and fibrils.

Results

To investigate binding, diffusion, and cleavage of MMP1 on native collagen, we followed the motion of individual fluorescently labeled MMP1 molecules bound to collagen fibrils abraded from a rat tail onto a quartz slide. The trajectories of individual molecules of activated wild-type (WT) MMP1 and its inactive mutant (E219Q) were extracted from movies recorded with 12 ms time resolution via prism-type TIRFM [28, 29] (Figures 1A–1C).

MMP1 Undergoes Cleavage-Dependent Biased and Hindered Diffusion

Individual MMP1 molecules moved along the long axis of the collagen fibril displaying virtually no motion across the fibril (Figures 1B and 1C; Figures S1A–S1C available online). The motion was characterized by calculating the mean square displacement (MSD) [30] as a function of time (Figure 1D). Fitting the MSD with the function 2Dt returned a diffusion constant D = 0.70 ± 0.01 $\mu m^2 s^{-1}$, which is in close agreement with D = 0.8 ± 0.2 $\mu m^2 s^{-1}$ from FCS experiments [17]. Over the initial ~0.5 s, the MSD of the WT MMP1 at 37°C was hindered compared to the mutant enzyme. At longer times, the curvature turned positive, consistent with biased motion (Figures 1D, S1D, and S1E; see Figure S1D for the method of quantifying hindrance and bias). Hindrance and bias decreased at 32°C, while at 20°C the MSD remained linear over the observation period, consistent with pure diffusion (Figures 1D, S1D, and S1E). The MSDs of the inactive MMP1 mutant (Figure 1D) and MMP9 (Figure S1C), neither of which is capable of cleaving native type I collagen fibrils, were linear at all temperatures.

Because both hindrance and bias depend on MMP1 activity, we hypothesized that cleavage of the substrate introduces a barrier that MMP1 is unable to cross. The barrier would bias the motion of the enzyme to one side of the cleavage site and hinder subsequent enzymes from crossing the cleaved site in either direction. We tested this hypothesis by following the diffusion of mutant MMP1 at 20°C on collagen pretreated with increasing concentrations of unlabeled wild-type MMP1 at 37°C (Figure 1E). The resulting MSD of the mutant MMP1 was well described by hindered diffusion without a biased component and, as expected, the extent of

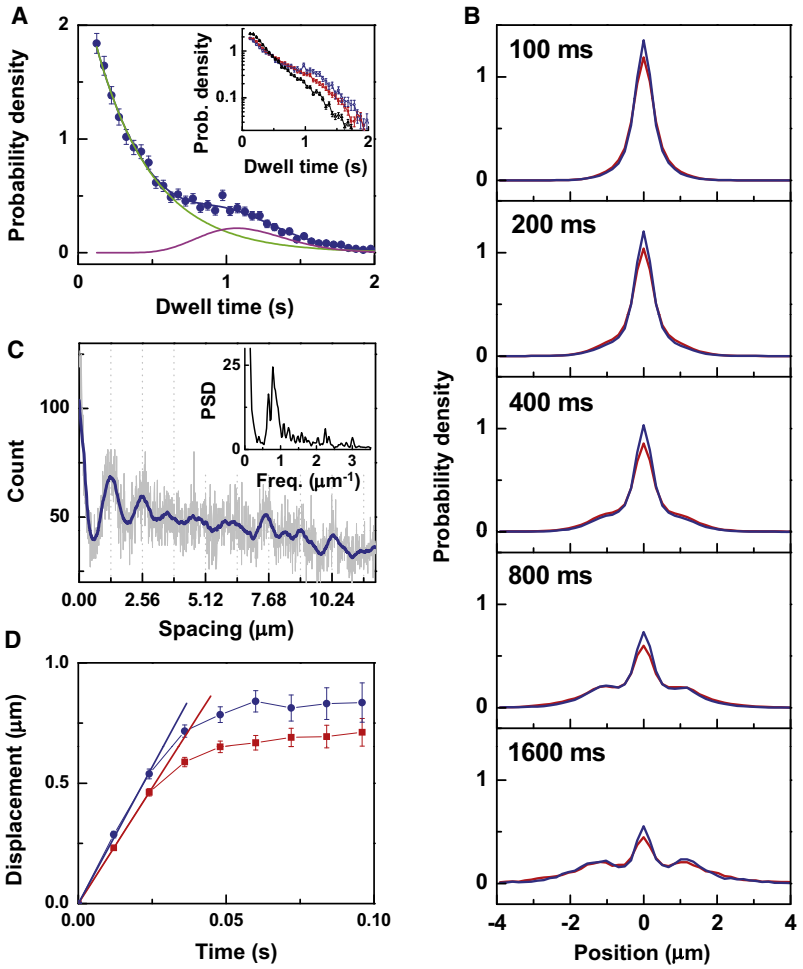

Figure 2. Characterization of MMP1 Motion

(A) Dwell time distribution for WT MMP1 at 37°C (blue closed circles, n = 6,627) fit to the sum (blue line) of an exponential (green line) and a gamma distribution (magenta line). Inset: Dwell time distributions of MMP1 (blue circles), mutant MMP1 (red squares, n = 15,733), and MMP9 (black triangles, n = 35,768) at 37°C. Error bars represent the statistical uncertainty from counting statistics.

(B) The time evolution of the displacement probability distribution for WT (blue line) and mutant (red line) MMP1 on collagen fibrils at 37°C. Note the two peaks that arise in the DPD at ±1.3 μm beginning at a time interval of 400 ms.

(C) Distribution of the pair-wise distances between the long (>0.8 s) class II pauses along the collagen fibril for WT MMP1 at 37°C. The blue line is the adjacent average over 40 points. The dotted lines correspond to a spacing of 1.3 μm. The power spectrum of the pair-wise distance distribution (inset) has two closely spaced dominant peaks at 0.64 and 0.78 μm^{-1} corresponding to intervals of 1.5 and 1.3 μm, respectively.

(D) Average displacement after pauses greater than 0.8 s for WT MMP1 at 37°C (blue closed circles) and mutant MMP1 (red closed squares). The straight lines correspond to linear fits of the first three points of the motion of WT MMP1 (blue) and mutant MMP1 (red) with slopes of 22.7 ± 0.4 and 19.3 ± 0.04, respectively. The error bars are the standard error of the mean.

See also Figure S2.

hindrance depended on the incubation time and the concentration of WT MMP1 during pretreatment. Hindrance did not result from a crowding effect as shown by the fact that pretreatment with unlabeled mutant enzyme under identical conditions had no effect on the MSD.

MMP1 Spends the Majority of Time in One of Two Distinct Pause States

To investigate enzyme motion and biased diffusion in greater detail, the trajectories of individual MMP1 molecules were subjected to a t test-based "step-finder" analysis [31]. Locations of the steps were used to fit the entire trajectory with a sequence of dwells and runs, from which the statistics of the motion, such as the duration of the dwells, were obtained (Figure 1B). MMP1 spent the majority of the time (90% ± 3%) paused on the collagen fibrils. The pausing behavior is reflected in the dwell time distribution (Figure 2A). At 37°C both WT MMP1 and the inactive mutant displayed two distinct dwell time distributions; a single exponential decay consistent with a first order pause escape rate of 2.5 ± 0.1 s^{-1} (class I pauses) and a symmetric distribution centered at 1.1 ± 0.3 s (class II pauses) (Figure 2A). The symmetric distribution is inconsistent with an exponential process or a sum of exponential processes but is well fit by a gamma distribution, which describes a process that includes multiple sequential kinetic steps of comparable rates [32, 33]. For a pause escape process with *n* identical irreversible steps of rate *k*, the dwell times would follow a gamma distribution centered at n/k. If the forward rates are similar, rather than identical, and the reverse rates are slow in comparison to the forward rates, there will no longer be a strict correspondence between the fitted gamma distribution parameters and the actual number of steps in the process. The symmetrically distributed dwell times present in both the WT and mutant MMP1 dwell time distributions were fit by a gamma distribution with n = 13 ± 3 and k = 15 ± 4 s^{-1} (Figures 2A and 3A–3C), suggesting that the enzyme escapes these class II pauses via multiple sequential kinetic steps of comparable rates and slow reverse rates. In contrast, the dwell time distribution for MMP9 was dominated by a single exponential decay rate of 3.06 ± 0.02 s^{-1} without the symmetrically distributed class of long pauses (Figure 2A, inset). The dwell-time distributions were similar for both WT and mutant MMP1 enzymes at 20°C, 32°C, and 37°C, but the gamma distributed pause amplitude increased ~2-fold between 20°C and 37°C for both enzymes, suggesting that entry into the gamma distributed class II pause state is temperature dependent (Figures 3A–3C). It is important to note that the gamma distribution is a two-parameter approximation of an undoubtedly more complicated process. Nonetheless, the pause escape process involves several, probably more than ten, steps with comparable forward rates and slow but finite backward rates.

MMP1 Preferentially Pauses at "Hot Spots" Periodically Spaced at 1.3 and 1.5 μm Intervals along Collagen Fibril

To characterize the spatial distribution of the pauses, the displacement probability distributions (DPD) were determined for different time intervals (Figure 2B). The DPD of purely diffusive motion is a Gaussian with a standard deviation

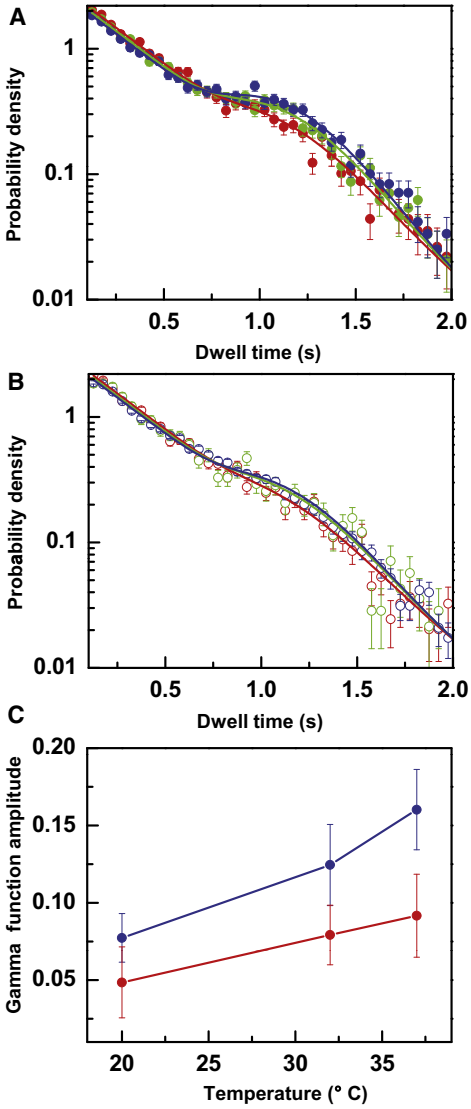

Figure 3. Temperature Dependence of Pausing for WT MMP1 and Mutant MMP1

(A) Pause dwell time distributions for WT MMP1 at 20°C (red circles), 32°C (green circles), and 37°C (blue circles).

(B) Pause dwell time distributions for mutant MMP1 at 20°C (open red circles), 32°C (open green circles), and 37°C (open blue circles).

The lines in (A) and (B) are a global fit to all six pause dwell time distributions with the sum of an exponential decay and a gamma distribution:

$$y(t) = a_1 e^{-k_1 t} + a_2 \left(\frac{k_2^n}{\Gamma(n)}\right) t^{n-1} e^{-k_2 t}$$

where the second term is the gamma distribution with n processes of rate k_2 and $\Gamma(n)$ is the gamma function, which for integer n > 0 is given by $(n-1)!$. Global fitting was done under the assumption that the exponential decay (k_1), the number of processes (n), and their rate (k_2) of the gamma distribution were the same for all conditions whereas the relative amplitudes of the exponential (a_1) and gamma distribution (a_2) were allowed to vary independently. The global fit parameters were as follows: $k_1 = 2.5 \pm 0.1\ s^{-1}$, n = 13 ± 4, and $k_2 = 15 \pm 4\ s^{-1}$ (errors in k_1, n, and k_2 represent the standard deviation of the fit parameters). Error bars represent uncertainties derived from counting statistics.

(C) The fraction of class II pauses as a function of temperature for WT MMP1 (blue dots) and mutant MMP1 (red dots), with lines as a guide to the eye. WT MMP1 consistently enters class II pauses more frequently than mutant MMP1 at each temperature, but the probabilities for both enzymes increase ~2-fold as the temperature increases from 20°C to 37°C. Error bars represent the standard deviation of the fit parameters.

proportional to the product of the time interval and the diffusion constant (Figure S4E). For short time intervals, the distributions were approximately Gaussian; however, two symmetric peaks centered near ±1.3 μm became apparent for time intervals greater than 400 ms. These peaks in the DPDs are consistent with long-lived, high-probability pauses spaced at ~1.3 μm intervals on the fibril and corroborate the class II pauses observed in the dwell time distributions (Figure 2A). Interestingly, these additional peaks were not as apparent in the DPDs for MMP9, suggesting that the pauses are enzyme specific (Figure S2A).

To accurately determine the spatial distribution of the class II pauses evident from the DPDs, we calculated the spacing along the fibril axis between each pair of pauses longer than 0.8 s (see the dwell time distribution in Figure 2A) from all of the MMP1 trajectories on each fibril at 37°C. The distribution of the long pause separations (Figure 2C) is consistent with a periodicity of ~1.3 μm. The power spectrum of the distribution (Figure 2C, inset) revealed two pronounced, closely spaced peaks at 0.64 μm^{-1} and 0.78 μm^{-1}, corresponding to spatial periods of 1.5 ± 0.2 μm and 1.3 ± 0.2 μm, respectively. Identical periods were obtained for mutant MMP1 at 37°C (Figure S2C). In contrast, the spacing between class I pauses (operationally defined as pauses less than 0.8 s) was not as periodic, and the small periodic component did not correspond to the spacing of the class II pauses (Figure S2D). These results are consistent with the motion of the individual MMP1 enzymes observed in the DPDs (Figure 2B). Together, these results suggest that class II pauses occur at periodically spaced susceptible sites or "hot spots" along the fibril. This periodicity, which has not been observed previously in structural measurements, is difficult to explain without an underlying structural feature of the collagen fibril being exposed by MMP1 binding. These sites may arise from the structural architecture of the fibril, e.g., a slight helical pitch of the microfibrils resulting in the periodic exposure of MMP1 binding sites at the surface of the fibril or differences in the stability or accessibility of these sites that arise during the directed self assembly of collagen fibrils. However, the temperature dependence of the probability of entering class II pauses supports a model in which the susceptible sites can locally unfold or "breathe" and are preferentially exposed by thermal fluctuations. The temperature dependence of the class II pauses, coupled with the fact that the WT MMP1 displayed a ~2-fold higher probability than the mutant enzyme of entering the class II pause (Figure 3), suggests that the class II pauses may be a precursor to collagenolysis.

Fiber Degradation Is Initiated after Class II Pauses and Results in Directional Motion

From the positive curvature in the MSDs of WT MMP motion on collagen fibrils (Figure 1), we infer that some portion of the motion is directionally biased by the cleavage process. To understand the origin of this biased motion and its connection to collagenolysis and the class II pauses, we examined the motion of the enzyme immediately after escaping from the long class II pauses. After pauses longer than 0.8 s, WT MMP1 moved faster and farther on average than did the mutant enzyme (Figure 2D). WT MMP1 escaped class II pauses at an average apparent speed of 11.8 ± 0.6 μm s^{-1} (mean ± SEM), significantly faster than that of mutant MMP1 (9.5 ± 0.4 μm s^{-1}). This increase in initial speed and displacement was specific to the class II pauses, as shown

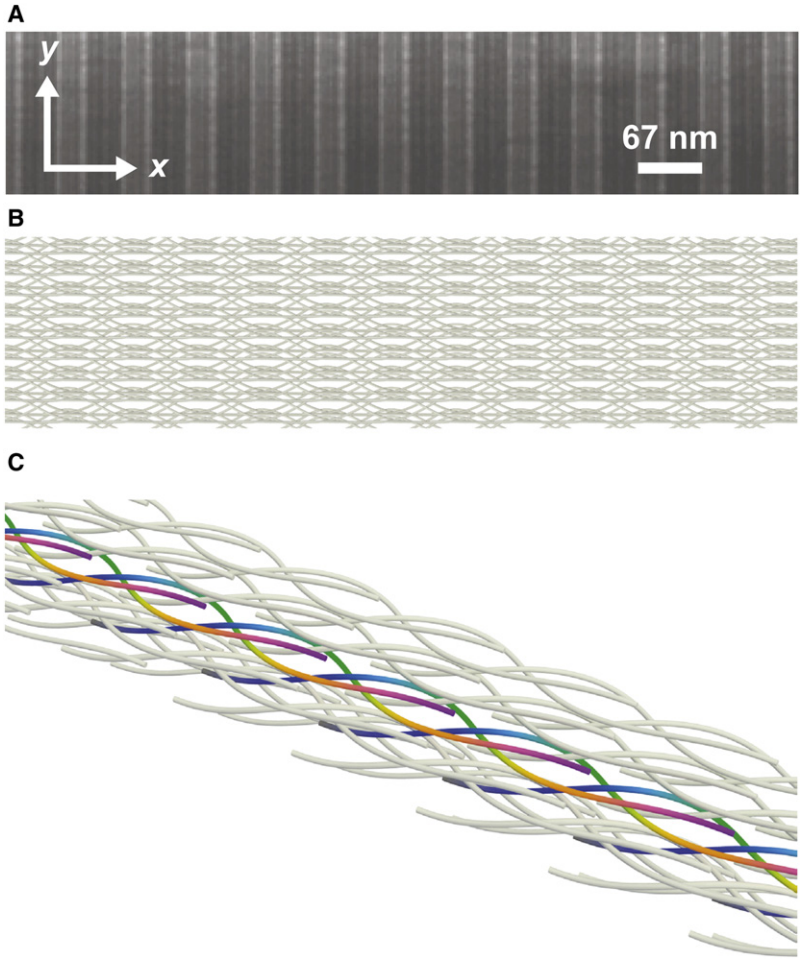

Figure 4. Collagen Fibril Organization

(A) TEM image of a typical type I collagen fibril used in the experiment.

(B) Two-dimensional view of the organization of collagen fibril based on the microfibrillar structural model of collagen [34].

(C) Three-dimensional view of the organization of collagen fibril in which individual 300 nm collagen monomers can be seen intertwined with one another. One microfibril that is made up of five collagen monomers (colored dark purple at the N terminus to light purple at the C terminus) is shown in the context of other microfibrils (gray).

See also Figure S3.

by the fact that there was no difference between the average motion of WT and mutant MMP1 at 37°C after pauses greater than 0.1 s, i.e., both class I and II pauses (Figure S4G). The increase in speed and magnitude of displacement after class II pauses is consistent with biased motion resulting from collagen cleavage by MMP1. We further expect that the bias should be directional, i.e., that each cleavage will bias the motion in the same direction along the fibril. To probe this hypothesis, we assigned a direction to each collagen fibril by averaging the displacements of all the tracked enzymes on the particular fibril in each direction after class II pauses. The first three points of the average displacements in each direction after a long pause were fit with a straight line to calculate the initial apparent velocity. For each fibril, the direction with the higher initial velocity was assigned as the positive direction. For mutant MMP1 at 37°C, the initial velocity for all of the fibrils in both directions was the same (16 ± 1 $\mu m\ s^{-1}$ and 15 ± 1 $\mu m\ s^{-1}$). The initial velocity for WT MMP1 at 37°C in the negative direction was indistinguishable from that of the mutant enzyme (16 ± 2 $\mu m\ s^{-1}$), but the average velocity in the positive direction was significantly faster (22 ± 2 $\mu m\ s^{-1}$). These results provide direct evidence of cleavage-dependent directionally biased motion that was inferred from the curvature in the MSD curves. Together, these results suggest that MMP1-induced cleavage is initiated after class II pauses and results in directionally biased motion along the collagen fiber.

Representation of Collagen Fibril Organization

To understand the physical basis of the cleavage process, we generated a three-dimensional representation of the organization of collagen monomers in a fibril based on the reported microfibrillar structure [34] (Figures 4B, 4C, and S3A–S3C). The resulting structure (Figure 4B) reproduces the D-period observed in the TEM images of rat tail type I collagen fibrils (Figure 4A). This representation provides a structural basis for the increased stability of fibrillar collagen, as the C-terminal end of each monomer occludes the MMP1 cleave site of the subsequent monomer [34]. Furthermore, this structural organization supports a collagen fibril degradation model in which initial cleavage is slow due to the inaccessibility of the cleavage sites, but once initiated, cleavage progresses rapidly as removal of the C-terminal end of one collagen monomer exposes the cleavage site of the next monomer [34] (Figure 5A). The collagen fibril degradation model is consistent with our observations of a slow initial cleavage followed by a rapid unidirectional motion along the fiber. In the context of the structural representation, directional motion associated with cleavage is in the N to C direction along the fibril. Simulations of diffusion between and cleavage of sites spaced by 67 nm, as described below, reproduces the increase in initial velocity observed for WT MMP1 (Figure S4B).

Collagen Fibril Degradation Model

Based on our experimental results, we propose a model in which both the WT and mutant enzymes diffuse on the surface of a collagen fibril but spend the majority of the time (~90%) in two distinct pause states. Class I pauses are random, temperature independent, and best described by a single exponential with an escape rate of 2.5 ± 0.1 s^{-1}. Class II pauses are periodically spaced at 1.3 ± 0.2 and 1.5 ± 0.2 μm intervals along the fibril and are temperature dependent. The dwell time distribution of class II pauses is symmetric and centered around 1.1 ± 0.3 s, implying multistep escape kinetics that can be approximated by a gamma distribution with 13 ± 3 sequential kinetic steps, each with a rate of 15 ± 4 s^{-1}. After a class II pause, the WT enzyme travels faster and farther, compared to the mutant enzyme, due to repetitive collagenolysis. Collagenolysis biases the diffusion of the WT enzyme and creates barriers that hinder the subsequent diffusion of enzymes on the fibril.

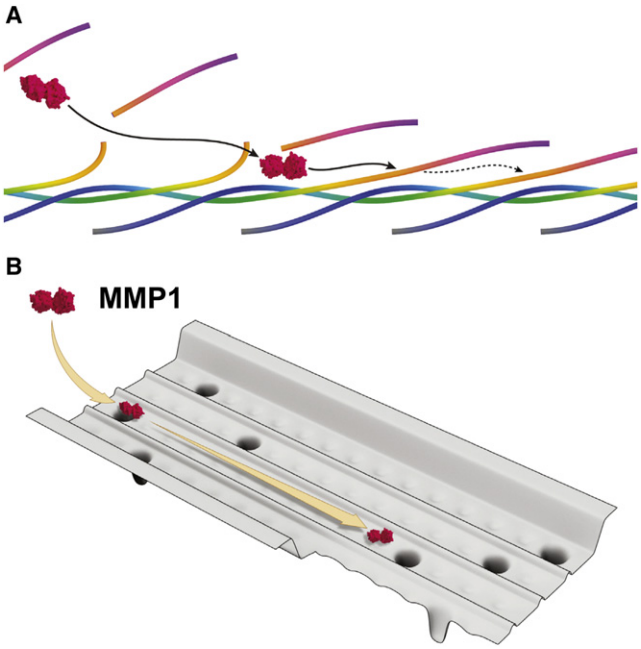

Figure 5. Model of Fibril Cleavage by MMP1

(A) Mechanism of cleavage. The cleavage site is located at the junction between the gold and purple segments of the collagen monomer. The cleavage site of each monomer is covered by the C-terminal end of the preceding monomer [34] (light purple). Once cleavage is initiated by MMP1 (purple), the cleaved C-terminal end is lost, exposing the subsequent cleavage site, thereby permitting rapid and processive cleavage of the successive monomers.

(B) Model potential energy landscape encountered by MMP1 (purple) as it diffuses on the collagen fibril. Microfibrils are separated by potential barriers. The short and long pause sites are represented by shallow, uniformly spaced potential wells and deeper potential wells spaced at ~1.3 μm intervals along the microfibrils, respectively.

Simulations of Collagen Fibril Degradation Model Reproduce Experimental Results

We generated trajectories of both WT and mutant MMP1 by computer simulations to test the collagen fibril degradation model. Simulated trajectories were analyzed in the same manner as the experimental trajectories and the experimental and simulation results were compared. The motion of MMP1 was modeled as one-dimensional diffusion modified by interactions with the collagen fibril and biased diffusion associated with cleavage (Figures 5A and 5B). The potential energy landscape (Figure 5B) consisted of one-dimensional tracks separated by potential barriers, reflecting the low probability of lateral motion. The tracks had weak pause sites every 67 nm, corresponding to low probability, nonspecific binding from which the enzyme escapes via a single kinetic step. Strong binding sites were spaced at 1.3 μm intervals, corresponding to the hot spots from which MMP1 could escape by either a single kinetic step or a multistep process suggested by the gamma distribution of class II pauses. Mutant MMP1 diffused through this landscape, whereas WT MMP1 could initiate cleavage of the substrate with low probability after class II pauses. A fraction of the class II pauses culminated in collagen cleavage by WT MMP, after which enzyme diffusion was restricted to one side of the cleaved substrate. This results in biased motion through the so-called burnt bridge Brownian ratchet [17, 35]. Subsequent to the initial cleavage, cleavage proceeds rapidly because the cleavage site of each successive monomer is exposed as the C-terminal end of the proceeding monomer is cleaved (Figure 5A). This model was adopted because simulations suggest that a single cleavage results in a local bias that does not affect the velocity or extent of the motion over an extended distance (Figures S4B and S4C). The increase in velocity and average displacement after class II pauses for the WT enzyme is therefore consistent with a model in which MMP1 cleaves several collagen monomers in rapid succession (Figures S4A–S4C). The simulation parameters were obtained from analyses of the single-molecule trajectories and were tuned to maximize agreement between the simulated and measured parameters. Details of the simulation are provided in Experimental Procedures and the simulation parameters are given in Table 1. The simulations reproduced the salient features of the experimental data (Figures 6A–6D) and led to insights not directly apparent from the data. The intrinsic diffusion coefficient for MMP1 on collagen fibrils was determined to be 7.5 ± 1 $\mu m^2 s^{-1}$, significantly larger than the apparent D measured by FCS (0.8 ± 0.2 $\mu m^2 s^{-1}$) [17] or MSD (0.70 ± 0.01 $\mu m^2 s^{-1}$). The 10-fold increase over the measured diffusion constant results from frequent pauses of MMP1. The average diffusion measured in the MSD curves is dominated by the pausing behavior of MMP1, which masks the much larger intrinsic diffusion constant. From the simulation results, we suggest that 40% ± 15% of the pauses at the hot spots are class II pauses and that 5% ± 2% of the class II pauses result in the initiation of cleavage, followed by 15 ± 4 successive cleavage events.

Simulations were run assuming either the canonical spacing of 300 nm between cleavage sites and a 67 nm stagger between the cleavage sites on the adjacent fibrils, or 67 nm between cleavage sites and no stagger between the cleavage sites on the adjacent fibrils, corresponding to the recently proposed microfibrillar organization (Figures 4 and 5A) [34]. Simulations with 67 nm cleavage spacing globally fit the data much better than the canonical 300 nm spacing. More specifically, the simulations reveal that the canonical 300 nm spacing between successive cleavage sites is not consistent with the observed increase in the average rate and extent of displacement (Figures S4A and S4D). However, the observed behavior is consistent with biased diffusion between, and rapid cleavage of, sites separated by 67 nm on the surface of the collagen fibril (Figures S4A–S4C).

Discussion

Single-molecule tracking of fluorescently labeled MMP1 molecules in combination with simulations provides a detailed picture of the complex MMP-native fibril interactions and insights into the mechanism of collagenolysis and the structure of fibrillar collagen. MMP1 undergoes biased and hindered diffusion in essentially one dimension along the collagen fibril without noticeable dissociation from the fibril. MMP1 spends 90% ± 3% of the time paused on the fibril in two distinct classes of pauses. Class I pauses occur randomly on the fibril with an escape rate of 2.5 ± 0.1 s^{-1}. Class II pauses are temperature dependent, occur at hot spots periodically spaced at 1.3 ± 0.2 and 1.5 ± 0.2 μm intervals along the fibril, and are well described by gamma distribution that arises from a complex pause escape pathway with 13 ± 3 sequential kinetic steps, each with a forward rate of 15 ± 4 s^{-1} and slow reverse rates [32, 33]. Class II pauses occur only at the hot spots, but they represent only 40% of the pauses at

Table 1. Simulation Parameters

Parameters		Values and Significance
Collagen Fibril Structure		
1	Cleavage site spacing	67 nm (either 67 or 300 nm)
2	Stagger	0 nm (either 0 or 67 nm)
3	Hot spot spacing	1.2 μm, defines the peak in DPDs at ~1.3 μm
4	Hot spot spacing SD	335 nm
5	Precleaved sites	1.35%, determines downward curvature of MSD, only for active WT enzyme
6	Adjacent track lateral spacing	3 nm (not varied)
Diffusion Constants		
7	1D diffusion constant (D)	7.5 ± 1 $\mu m^2 s^{-1}$, intrinsic diffusion constant
8	Lateral jump rate (P_j)	0.5 s^{-1}, rate of jumping to adjacent tracks
MMP1 Binding Properties		
9	Binding to regular sites	150 s^{-1}
10	Binding to hot spots	30,000 s^{-1}
11	Type I pause escape rate	5 s^{-1}
12	Number of kinetic steps in type II (gamma) pause	11 ± 3 steps
13	Rate of kinetic steps in type II pause	11 ± 3 s^{-1} (the average lifetime of the type II pauses is ~1 s)
14	Fraction of class II pauses at hot spots	40% ± 15% (WT), 5% ± 5% (mutant), fraction of hot spot pauses that escape via gamma distribution
MMP1 Cleavage Properties		
15	Percentage of cleavage after long dwells	5% ± 2%
16	Number of successive cuts after initial cut	15 ± 4, determines upward curvature of MSD and average motion after a long pause
17	SD of number of cuts	3, reflects intrinsic variability in the number of successive cuts, which is a Gaussian distribution centered at 15 cuts with a standard deviation of 3.
Additional Simulation Parameters		
18	Noise (σ_x)	170 nm, determines y-intercept of MSDs
19	Time step (Δt)	1 μs, simulation time step (not varied)

The parameters of the simulation, organized by category, are listed along with their values as determined from minimizing the discrepancies between the experimental and simulation results. The uncertainties in the simulation parameters were estimated by varying the parameter and comparing the results with the experimental data, as described in Experimental Procedures.

the preferential hot spot locations; the remaining 60% of the pauses are the short class I pauses. For WT MMP1 at 37°C, 5% ± 2% of the class II pauses result in the initiation of cleavage, followed by rapid and processive cleavage of 15 ± 4 collagen monomers. Although cleavage could not be directly observed in individual trajectories of MMP1 motion, it could be inferred from the bias observed in the MSD curves and more specifically in the unidirectional increase in the velocity and extent of motion after class II pauses. Since the cleavage reaction was observed from the statistics of the motion, the quantitative details of the process including the percentage of productive long pauses (5% ± 2%), the number of processive cleavages (15 ± 4), and the fraction of class II pauses at the hot spots (40% ± 15%) were obtained from simulations. The motion of WT MMP1 at 32°C could be reproduced by slightly modifying only two of the simulation parameters (the amount of precleavage and the fraction of class II pauses at hot spots) obtained for WT MMP1 at 37°C (Figure S4F).

The temperature-dependent pausing of MMP1 on native fibrils at specific locations suggests a possible explanation for the remarkable temperature dependence of fibril degradation. Local unfolding or "breathing" of the collagen fibril at the hot spots on the fibril makes otherwise resistant fibrils vulnerable to collagenolysis. However, the low probability of cleavage after class II pauses implies that pausing at these sites is necessary but not sufficient to initiate collagen degradation. The large activation energy of collagen fibril degradation [18] suggests that subsequent steps in the cleavage process are also temperature dependent and that the overall activation energy results from the multiplicative effect of several temperature-dependent processes, including entry into the class II pause state.

The class II pause state has not previously been observed in the cleavage of collagen monomers or fibrils. From our findings we posit that the class II pause state corresponds to the progressive melting or rearrangement of collagen at specific susceptible sites that expose the cleavage site. This process is distinct from melting or rearrangement of the three polypeptide chains in the collagen monomer required for cleavage [21, 22, 36], because cleavage proceeds rapidly once initiated (Figure 2D) and the pause kinetics are similar for both WT and catalytically inactive mutant MMP1 enzymes (Figures 3A–SC). Within the context of the structural of fibrillar collagen [34], class II pauses can be associated with the process of initiating degradation that requires melting or disruption of the C-terminal end of the occluding collagen monomer (Figures 5A and S3C). The precise biochemical or structural basis for the periodic arrangement of sites at which MMP1 binds and initiates this process is presently unknown, but it does suggest a possible regulatory mechanism for collagen degradation. Modifying the location or affinity of the pause sites at which degradation is licensed would dramatically alter the susceptibility of the fibrils to MMP degradation. Because the bursts of degradation occur after escape from the kinetically complex pauses, the duration of the pause and the efficiency of initiating degradation after escape from the pause are also potential points of regulation. Moreover, because the class II pause is an obligate state on the

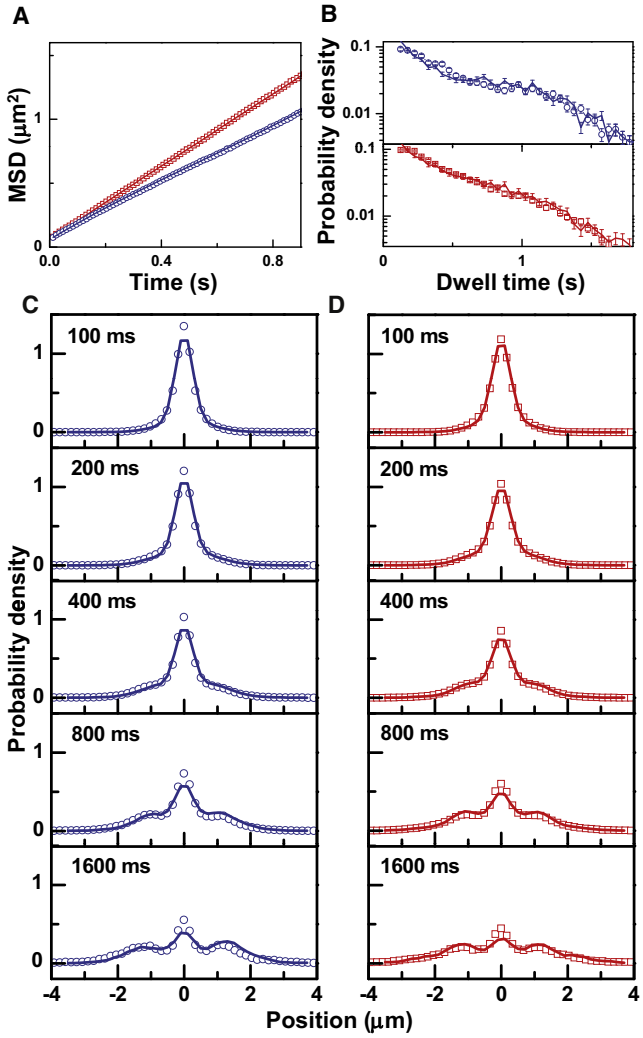

Figure 6. Comparison between Simulations and Experiment

(A) MSDs of the experimental data for WT MMP1 (blue circles) and mutant MMP1 (red squares) are well described by the simulation results (blue and red lines, respectively).

(B) Dwell time distributions for WT MMP1 (blue circles) with simulation results (blue line) and for mutant MMP1 (red squares) with simulation results (red line).

(C and D) Displacement probability distributions for WT MMP1 (blue circles) and the simulation (blue line) (C), and for mutant MMP1 (red squares) and the simulation (red line) (D).

Error bars in (A) and (B) represent the standard error of the mean. See also Figures S4B–S4F.

degradation pathway, the overall rate of degradation is sensitive to the kinetics of the pause state, which presents an additional powerful means of regulation.

The average cleavage rate estimated from analysis of the single-molecule trajectories was $\sim$0.3 s^{-1} $MMP1^{-1}$ at 37°C (see Experimental Procedures), which is in reasonable agreement with values obtained from ensemble measurements of collagen fibril degradation by MMP1 [18, 37, 38] of 0.005 s^{-1} $MMP1^{-1}$ at 25°C, which gives a rate of $\sim$1 s^{-1} $MMP1^{-1}$ at 37°C when corrected for the large activation energy of collagen fibril degradation [18]. The degradation process of native collagen is dominated by binding, diffusion, and pausing behavior of MMP1 rather than the kinetics of collagen cleavage, which appear to be rapid in comparison with the remaining steps in the process. The dramatic decrease in cleavage of fibrillar collagen as compared with the triple helical collagen monomer and gelatin arises from the fact that MMP1 bound to native collagen spends the majority (90% ± 3%) of the time in inactive pause states and initiates cleavage with low probability (5% ± 2%) only at specific vulnerable sites spaced at 1.3 ± 0.2 and 1.5 ± 0.2 μm intervals. The cleavage reaction is further reduced by the increasing barriers to diffusion that accompany degradation of the collagen fibril coupled with the low probability of lateral motion between the adjacent collagen fibrils. These effects collectively slow the diffusion of MMP1 as the degradation proceeds. This self-limiting behavior is counterbalanced by the rapid and processive burst of 15 ± 4 cleavage events after the initiation of cleavage. Thus, the mechanism of molecular collagen degradation is significantly different from that of fibril degradation. The spatial distribution of hot spots spaced at 1.3 ± 0.2 and 1.5 ± 0.2 μm intervals was unanticipated and from this we infer the existence of a higher-order periodic structural or biochemical modification of type I collagen that renders it susceptible to binding and cleavage by MMP1 with a characteristic length scale $\sim$4-fold longer than the 300 nm collagen monomer length. The combination of experiments, modeling, and simulations provides a clear picture of native collagen fibril degradation and our approach is readily applicable to other types of collagen fibrils and MMPs. More generally, these results demonstrate the importance of enzyme motion on, and interactions with, an extended substrate in determining the overall catalytic rate.

Experimental Procedures

Preparation of Rat Tail Collagen Fibrils

Rat tails from animals sacrificed in unrelated experiments and frozen were procured from Washington University Animal Facility and stored at −80°C. Tendon bundles were exposed after removal of tail skin and sheath and disrupted mechanically over aldehyde activated quartz microscope slides (CEL Associates Inc, Pearland, TX) until abraded individual fibrils were clearly visible in the microscope. After the slides were cleared of debris and larger tendon bundles, individual fibrils remained attached to the activated glass. The glass was then blocked by submersion in blocking solution consisting of 50 mM Tris-HCl (pH 7.5) buffer containing 50 mM NaCl and 2 mg/ml BSA overnight at 4°C.

Enzyme Purification, Labeling, and Activation

MMP1, along with its active center mutant "E219Q," and MMP9 proenzymes were purified from serum-free conditioned medium of p2aHTA cells stably transfected with the corresponding cDNAs as described previously [17, 38]. MMP1 was labeled with Alexa 488 or Alexa 555 fluorescent dye with the Alexa Fluor Protein labeling kit (Molecular Probes; A-10235 and A-20174, respectively) as described [17]. The MMP9 Enzyme (50 μg) was absorbed onto a column (100 μl bed volume) of Gelatin Agarose resin (Sigma G-5384, Sigma-Aldrich Chemical Co.), equilibrated with 25 mM HEPES buffer (pH 8.0), containing 2 mM $CaCl_2$ and 50 mM NaCl. The loaded resin was incubated with Alexa 488 dye for 30 min at room temperature. The enzyme was eluted with the same buffer containing 10% DMSO and dialyzed against 6 mM Tris (pH 7.5) buffer containing 0.5 mM $CaCl_2$, 25 mM NaCl, and 0.001% Brij-35. The eluted enzyme was concentrated $\sim$4-fold by limited evaporation. The labeling conditions were adjusted to yield an enzyme with 1.0 mole of Alexa 488 per mole of enzyme. Activation of the labeled enzymes was performed immediately prior to an experiment. MMP1 was activated with plasmin and stromelysin 1 (MMP3), as described [17]. MMP9 was activated by addition of plasmin to achieve 10:1 molar ratio. The enzyme mixture was incubated for 1 hr at 37°C and the plasmin activity was inhibited by addition of a 5-fold molar excess of aprotinin.

Enzyme Activity Assay

Activity of labeled and unlabeled WT MMP1 was tested with reconstituted collagen fibrils. Acetic acid (17.4 mM) soluble rat tail collagen was prepared

at a concentration of 2 mg/ml. Collagen fibrils were reconstituted from 50 μl of collagen solution to form turbid collagen gels in glass tubes of 6 mm internal diameter. Fibril reconstitution was initiated by neutralization of collagen solution to pH 7.5 with simultaneous heating to 37°C. Addition of 1 μg of MMP1 activated with plasmin/MMP3 mixture [39, 40] to such gels resulted in complete dissolution of the collagen fibrils within an hour. The enzyme labeled with Alexa 488 at 1:1 molar ratio retained similar activity. Dissolution of the collagen fibrils does not occur with gelatinase or trypsin.

Transmission Electron Microscopy of Collagen Fibrils

A segment of abraded but not immobilized rat-tail collagen fibril was placed on a copper EM grid with 400 mesh and formvar/carbon coating. The EM grid was treated with glow discharge for 30 s in an EMScope TB500 (EMSCOPE Laboratories, England). The collagen fibril was stained with a drop of 0.5% aqueous uranyl acetate for 30 s after which the stain was removed with filter paper. The sample was imaged in a JEM-1200EX II transmission electron microscope (JEOL, Japan) with an AMT CCD camera system (Advanced Microscopy Techniques, Danvers, MA, USA).

Single-Molecule Measurements

Single-molecule measurements were made with a custom prism-type total internal reflection fluorescence microscope [41] based on an Olympus IX71. Measurements were made in 50 mM Tris (pH 7.5), 150 mM NaCl, and 1 mM $CaCl_2$. The excitation laser (~2.5 mW) was focused onto an area of ~150 μm × 150 μm. About 200 pM Alexa 555-labeled MMP1 was flowed into the flow cell. Labeled MMPs bound to collagen fibrils on the quartz slide were excited and the fluorescence was collected by an EMCCD camera (Andor DV897DCS-BV). Movies were recorded with 10 ms exposures, at a rate of 83.3 frames per second. Detailed procedures are as reported [42].

Calculation of Average Collagenolysis Rate for WT MMP1

To calculate the average rate of collagen fibril collagenolysis for WT MMP1 at 37°C, we considered the average behavior of all the individual enzymes. Comparing the total time of all the experimental trajectories (2,930 s) to the total time the enzymes were paused (2,725 s) suggests that the enzyme was paused 93% of the time. The average dwell time including both the class I and class II pauses was 0.43 s, from which we calculate an average of 2.3 pauses per second. Class II pauses account for approximately 20% of the total pauses, and approximately 5% of the class II pauses (from simulations) results in the cleavage of 15 monomers (from simulations). From these results, we calculate a cleavage rate of ~0.35 s^{-1} per enzyme.

Construction of a 3D Representation for the Organization of Collagen Monomers in a Fibril

A three-dimensional representation of the collagen fibril was constructed based on a previously reported microfibrillar structure [34]. Three-dimensional splines were projected through a series of 14 planar cross-sections (Figure S3), each separated by a distance of 67 nm, equivalent to the D-periodicity of collagen. Planes were laid out parallel to one another and spaced at 67 nm intervals along a projection line. Individual splines were then created for each collagen monomer by connecting consecutive intersection points 1–5 across a series of five planes (Figure S3). A smooth Bezier curve was applied to each vertex of the 3D spline to give the monomer a smooth appearance. Multiple instances of the original spline were cloned until each projection point throughout all 14 packing planes was filled. Note that there was one instance where two splines intersected. To compensate for this collision between neighboring monomers, one of the splines was minimally displaced laterally. Finally, volume was added to the splines by enabling radial (cylindrical) rendering in 3D Studio Max. The radial thickness was varied in order to enhance visualization of the organization of the collagen fibril. All visualization model building was performed in Autodesk 3D Studio Max (Autodesk Inc., San Rafael, CA).

Supplemental Information

Supplemental Information includes Supplemental Experimental Procedures (including additional details of data analyses, simulations, and fitting) and four figures and can be found with this article online at doi:10.1016/j.cub.2012.04.012.

Acknowledgments

We thank Sarah Hong for help with the EM images; Alan Hoofring for help with the artwork in Figures 4B, 4C, 5A, 5B, and S3C; Chris Combs for providing the tracking software; and Attila Szabo, Sergey Leikin, Joseph Orgel, and Elliot Elson for enlightening discussion. We thank Richard Neuman, Jon Silver, and Elliot Elson for comments on the manuscript. We thank Pacific Edit for help with editing our manuscript. This research was supported by the Intramural Research Program of the National Institutes of Health, NHLBI and grants R01AR040618 from NIAMS, NIH, and R01CA123363 from NCI, NIH to G.G.

Received: December 23, 2011
Revised: March 9, 2012
Accepted: April 2, 2012
Published online: May 10, 2012

References

1. Kreis, T., and Vale, R., eds. (1999). Guidebook to the Extracellular Matrix, Anchor and Adhesion Proteins, 2nd Edition (New York: A Sambrose and Tooze Publication at Oxford University Press).
2. Yurchenko, P.D., Birk, D.E., and Mecham, R.P., eds. (1994). Extracellular Matrix Assembly and Structure (San Diego: Academic Press, Inc.).
3. Page-McCaw, A., Ewald, A.J., and Werb, Z. (2007). Matrix metalloproteinases and the regulation of tissue remodelling. Nat. Rev. Mol. Cell Biol. *8*, 221–233.
4. Kessenbrock, K., Plaks, V., and Werb, Z. (2010). Matrix metalloproteinases: regulators of the tumor microenvironment. Cell *141*, 52–67.
5. Nagase, H., Visse, R., and Murphy, G. (2006). Structure and function of matrix metalloproteinases and TIMPs. Cardiovasc. Res. *69*, 562–573.
6. Brinckerhoff, C.E., and Matrisian, L.M. (2002). Matrix metalloproteinases: a tail of a frog that became a prince. Nat. Rev. Mol. Cell Biol. *3*, 207–214.
7. Adiguzel, E., Ahmad, P.J., Franco, C., and Bendeck, M.P. (2009). Collagens in the progression and complications of atherosclerosis. Vasc. Med. *14*, 73–89.
8. Murphy, G., and Nagase, H. (2008). Reappraising metalloproteinases in rheumatoid arthritis and osteoarthritis: destruction or repair? Nat. Clin. Pract. Rheumatol. *4*, 128–135.
9. Parks, W.C., Mecham, R.P., Deryugina, E.I., and Quigley, J.P. (2011). The role of matrix metalloproteinases in cellular invasion and metastasis. In Extracellular Matrix Degradation, *Volume 2*, W.C. Parks, ed. (New York: Springer), pp. 145–191.
10. Liotta, L.A., Tryggvason, K., Garbisa, S., Hart, I., Foltz, C.M., and Shafie, S. (1980). Metastatic potential correlates with enzymatic degradation of basement membrane collagen. Nature *284*, 67–68.
11. Han, S., Makareeva, E., Kuznetsova, N.V., DeRidder, A.M., Sutter, M.B., Losert, W., Phillips, C.L., Visse, R., Nagase, H., and Leikin, S. (2010). Molecular mechanism of type I collagen homotrimer resistance to mammalian collagenases. J. Biol. Chem. *285*, 22276–22281.
12. Minond, D., Lauer-Fields, J.L., Cudic, M., Overall, C.M., Pei, D., Brew, K., Visse, R., Nagase, H., and Fields, G.B. (2006). The roles of substrate thermal stability and P2 and P1′ subsite identity on matrix metalloproteinase triple-helical peptidase activity and collagen specificity. J. Biol. Chem. *281*, 38302–38313.
13. Minond, D., Lauer-Fields, J.L., Nagase, H., and Fields, G.B. (2004). Matrix metalloproteinase triple-helical peptidase activities are differentially regulated by substrate stability. Biochemistry *43*, 11474–11481.
14. Chung, L.D., Dinakarpandian, D., Yoshida, N., Lauer-Fields, J.L., Fields, G.B., Visse, R., and Nagase, H. (2004). Collagenase unwinds triple-helical collagen prior to peptide bond hydrolysis. EMBO J. *23*, 3020–3030.
15. Bertini, I., Fragai, M., Luchinat, C., Melikian, M., Toccafondi, M., Lauer, J.L., and Fields, G.B. (2012). Structural basis for matrix metalloproteinase 1-catalyzed collagenolysis. J. Am. Chem. Soc. *134*, 2100–2110.
16. Collier, I.E., Saffarian, S., Marmer, B.L., Elson, E.L., and Goldberg, G.I. (2001). Substrate recognition by gelatinase A: the C-terminal domain facilitates surface diffusion. Biophys. J. *81*, 2370–2377.
17. Saffarian, S., Collier, I.E., Marmer, B.L., Elson, E.L., and Goldberg, G. (2004). Interstitial collagenase is a Brownian ratchet driven by proteolysis of collagen. Science *306*, 108–111.
18. Welgus, H.G., Jeffrey, J.J., and Eisen, A.Z. (1981). Human skin fibroblast collagenase. Assessment of activation energy and deuterium isotope effect with collagenous substrates. J. Biol. Chem. *256*, 9516–9521.
19. Welgus, H.G., Jeffrey, J.J., and Eisen, A.Z. (1981). The collagen substrate specificity of human skin fibroblast collagenase. J. Biol. Chem. *256*, 9511–9515.

20. Welgus, H.G., Jeffrey, J.J., Stricklin, G.P., Roswit, W.T., and Eisen, A.Z. (1980). Characteristics of the action of human skin fibroblast collagenase on fibrillar collagen. J. Biol. Chem. *255*, 6806–6813.
21. Leikina, E., Mertts, M.V., Kuznetsova, N., and Leikin, S. (2002). Type I collagen is thermally unstable at body temperature. Proc. Natl. Acad. Sci. USA *99*, 1314–1318.
22. Nerenberg, P.S., Salsas-Escat, R., and Stultz, C.M. (2008). Do collagenases unwind triple-helical collagen before peptide bond hydrolysis? Reinterpreting experimental observations with mathematical models. Proteins *70*, 1154–1161.
23. Collier, I.E., Legant, W., Marmer, B., Lubman, O., Saffarian, S., Wakatsuki, T., Elson, E., and Goldberg, G.I. (2011). Diffusion of MMPs on the surface of collagen fibrils: the mobile cell surface-collagen substratum interface. PLoS ONE *6*, e24029.
24. Adhikari, A.S., Chai, J., and Dunn, A.R. (2011). Mechanical load induces a 100-fold increase in the rate of collagen proteolysis by MMP-1. J. Am. Chem. Soc. *133*, 1686–1689.
25. Camp, R.J., Liles, M., Beale, J., Saeidi, N., Flynn, B.P., Moore, E., Murthy, S.K., and Ruberti, J.W. (2011). Molecular mechanochemistry: low force switch slows enzymatic cleavage of human type I collagen monomer. J. Am. Chem. Soc. *133*, 4073–4078.
26. Rosenblum, G., Van den Steen, P.E., Cohen, S.R., Bitler, A., Brand, D.D., Opdenakker, G., and Sagi, I. (2010). Direct visualization of protease action on collagen triple helical structure. PLoS ONE *5*, e11043.
27. Sun, H.B., Smith, G.N., Jr., Hasty, K.A., and Yokota, H. (2000). Atomic force microscopy-based detection of binding and cleavage site of matrix metalloproteinase on individual type II collagen helices. Anal. Biochem. *283*, 153–158.
28. Axelrod, D., Burghardt, T.P., and Thompson, N.L. (1984). Total internal reflection fluorescence. Annu. Rev. Biophys. Bioeng. *13*, 247–268.
29. Trache, A., and Meininger, G.A. (2008). Total internal reflection fluorescence (TIRF) microscopy. Curr. Protoc. Microbiol., Chapter 2, 2A, 2, 1–2A, 2, 22.
30. Qian, H., Sheetz, M.P., and Elson, E.L. (1991). Single particle tracking. Analysis of diffusion and flow in two-dimensional systems. Biophys. J. *60*, 910–921.
31. Carter, N.J., and Cross, R.A. (2005). Mechanics of the kinesin step. Nature *435*, 308–312.
32. Chemla, Y.R., Moffitt, J.R., and Bustamante, C. (2008). Exact solutions for kinetic models of macromolecular dynamics. J. Phys. Chem. B *112*, 6025–6044.
33. Neuman, K.C., Saleh, O.A., Lionnet, T., Lia, G., Allemand, J.F., Bensimon, D., and Croquette, V. (2005). Statistical determination of the step size of molecular motors. J. Phys. Condens. Matter *17*, S3811–S3820.
34. Perumal, S., Antipova, O., and Orgel, J.P.R.O. (2008). Collagen fibril architecture, domain organization, and triple-helical conformation govern its proteolysis. Proc. Natl. Acad. Sci. USA *105*, 2824–2829.
35. Saffarian, S., Qian, H., Collier, I., Elson, E., and Goldberg, G. (2006). Powering a burnt bridges Brownian ratchet: a model for an extracellular motor driven by proteolysis of collagen. Phys. Rev. E Stat. Nonlin. Soft Matter Phys. *73*, 041909.
36. Nagase, H., and Fushimi, K. (2008). Elucidating the function of non catalytic domains of collagenases and aggrecanases. Connect. Tissue Res. *49*, 169–174.
37. Aimes, R.T., and Quigley, J.P. (1995). Matrix metalloproteinase-2 is an interstitial collagenase. Inhibitor-free enzyme catalyzes the cleavage of collagen fibrils and soluble native type I collagen generating the specific 3/4- and 1/4-length fragments. J. Biol. Chem. *270*, 5872–5876.
38. Goldberg, G.I., Strongin, A., Collier, I.E., Genrich, L.T., and Marmer, B.L. (1992). Interaction of 92-kDa type IV collagenase with the tissue inhibitor of metalloproteinases prevents dimerization, complex formation with interstitial collagenase, and activation of the proenzyme with stromelysin. J. Biol. Chem. *267*, 4583–4591.
39. Nagase, H., Suzuki, K., Enghild, J.J., and Salvesen, G. (1991). Stepwise activation mechanisms of the precursors of matrix metalloproteinases 1 (tissue collagenase) and 3 (stromelysin). Biomed. Biochim. Acta *50*, 749–754.
40. He, C.S., Wilhelm, S.M., Pentland, A.P., Marmer, B.L., Grant, G.A., Eisen, A.Z., and Goldberg, G.I. (1989). Tissue cooperation in a proteolytic cascade activating human interstitial collagenase. Proc. Natl. Acad. Sci. USA *86*, 2632–2636.
41. Roy, R., Hohng, S., and Ha, T. (2008). A practical guide to single-molecule FRET. Nat. Methods *5*, 507–516.
42. Hardin, A.H., Sarkar, S.K., Seol, Y., Liou, G.F., Osheroff, N., and Neuman, K.C. (2011). Direct measurement of DNA bending by type IIA topoisomerases: implications for non-equilibrium topology simplification. Nucleic Acids Res. *39*, 5729–5743.